4700 *Chem. Mater.* **2010,** *22,* 4700–4711
DOI:10.1021/cm100976q

CHEMISTRY OF MATERIALS
Article

# Conductivity Behavior of Composites in the $La_{0.6}Sr_{0.4}CoO_{3\pm\delta}$ - $CeO_2$ System: Function of Connectivity and Interfacial Interactions

Elena Konysheva,* Ross Blackley, and John T. S. Irvine

*School of Chemistry, University of St. Andrews, St. Andrews, Fife, KY 16 9ST, U.K.*

*Received April 8, 2010. Revised Manuscript Received June 29, 2010*

The electrical properties of a series of composites formed by reactive sintering have been investigated. Six composite samples with the same composition 43 mol % $La_{0.6}Sr_{0.4}CoO_{3\pm\delta}$· 57 mol % $CeO_2$ (LSCC57) were fabricated through mixing of the initial LSC and $CeO_2$ followed by milling of the mixture for different periods of time (up to 261 h) and fired at 1350 °C. According to X-ray diffraction (XRD), at room temperature all the LSCC57 composites are composed of the modified perovskite with rhombohedrally distorted perovskite structure ($R\bar{3}c$, no. 167) and modified ceria with fluorite structure ($Fm\bar{3}m$, no. 225). The modification of the initial phases takes place because of cross-dissolution of La, Sr, and Co from the initial LSC into the fluorite structure and Ce from the $CeO_2$ into the perovskite structure. Depending upon fabrication history these composites showed unusual conductivity behavior with strong reversible hysteresis between heating and cooling stages. The transport properties of the LSCC57 composites are determined by several factors: (i) good three-dimensional (3D) connectivity between grains of the most conductive phase (modified perovskite); (ii) recombination of holes (from the modified perovskite) and electrons (from the modified ceria) at phase interfaces could decrease electronic conductivity in the composite materials; (iii) existence of epitaxial coherence between oxygen sublattices at the {modified perovskite/modified ceria} interface could facilitate oxygen transport across the phase interfaces; and (iv) mechanochemical interactions during fabrication (mixing followed by milling) and during high temperature treatment. The transport properties of nanoscale phases at interfacial regions are thought to have strong influence on the conductivity of the LSCC57 composites, in particular, where the grains of the modified perovskite do not form a robust 3D continuous network through the composite material and lead to the appearance of the conductivity hysteresis with the temperature variation.

## 1. Introduction

Functional composite ceramics comprise two or more phases with different physical, transport, chemical, catalytic, or mechanical properties. Composite materials maintaining high electronic conductivity, sufficient ionic conductivity, and high catalytic activity are of great importance for application as electrodes in solid oxide fuel cells and batteries.[1−4] In general, percolation and effective media theories can be used to describe electrical properties, thermal conductivity, diffusion characteristics, and permeability of these composites.[5] The percolation threshold depends on the microstructure of materials: particle sizes and geometry of the initial components and their distribution through the volume.[5,6] Incorporation of a phase with distinct physicochemical properties into the matrix of another phase can allow the enhancement of existing functions within the initial matrix. This can be illustrated by number of experimental and theoretical studies carried out for the composite solid electrolytes LiX-$Al_2O_3$ (X = $I^-$, $F^-$, $Cl^-$, $Br^-$, $CO_3^{2-}$, $SO_4^{2-}$, and $PO_4^{3-}$), AgX-$Al_2O_3$ (X = $I^-$, $Cl^-$, and $Br^-$) or YSZ-$Al_2O_3$.[7−12] The enhancement of the ionic conductivity was attributed to the space−charge effect: the grain boundary contribution was diminished because of the presence of a surface active second phase (fine−grained insulating $Al_2O_3$ particles).[12] Addition of a phase with different physicochemical properties allows the introduction of new properties into an initial matrix. This is one of the reasons why composite ceramic materials have found wide applications for solving energy and environmental issues.[1−4,13,14]

*To whom correspondence should be addressed. E-mails: ek31@st-andrews.ac.uk, elena.konysheva@googlemail.com.

(1) Atkinson, A.; Barnett, S.; Gorte, R. J.; Irvine, J. T. S.; McEvoy, A. J.; Mogensen, M.; Singhal, S. C.; Vohs, J. *Nat. Mater.* **2004**, *3*, 17.
(2) Virkar, A. V.; Chen, J.; Tanner, C. W.; Kim, J. W. *Solid State Ionics* **2000**, *131*, 189.
(3) Prosini, P. P.; Zane, D.; Pasquali, M. *Electrochim. Acta* **2001**, *46*, 3517.
(4) Konysheva, E.; Mertens, J.; Penkalla, H.; Singheiser, L.; Hilpert, K. *J. Electrochem. Soc.* **2007**, *154*, B1252.
(5) McLachlan, D. S.; Blaszkiewicz, M.; Newnham, R. E. *J. Am. Ceram. Soc.* **1990**, *73*, 2187.
(6) Costamagna, P.; Costa, P.; Antonucci, V. *Electrochim. Acta* **1998**, *43*, 375.
(7) Liang, C. C. *J. Electrochem. Soc.* **1973**, *120*, 1289.
(8) Uvarov, N. F.; Isupov, V. P.; Sharma, V.; Shukla, A. K. *Solid State Ionics* **1992**, *51*, 41.
(9) Knauth, P. *J. Electroceram.* **2000**, *5*, 111.
(10) Feighery, A. J.; Irvine, J. T. S. *Solid State Ionics* **1999**, *121*, 209.
(11) Chung, R. W.; de Leeuw, S. W. *Solid State Ionics* **2004**, *175*, 851.
(12) Maier, J. *Nat. Mater.* **2005**, *4*, 805.
(13) Wang, D.; Zou, Z.; Ye, J. *Chem. Mater.* **2005**, *17*, 3255.
(14) Zhong, L. S.; Hu, J. S.; Cao, A. M.; Liu, Q.; Song, W. G.; Wan, L. J. *Chem. Mater.* **2007**, *19*, 1648.


Published on Web 07/21/2010

Unusual features could also appear within a composite matrix in the case of structural transformations, electronic, chemical or electrochemical interactions at the interface between initial components. Recently, an enhancement of ferroelectricity at metal/complex oxides interfaces in ultra-thin-film devices was reported.[15] In another example current induced mass transport of $WO_3$ (n-type conductor) in the anion form ($WO_4^{2-}$) was observed in the $CaWO_4/WO_3$ composite system.[16,17] In the present, ongoing study, conductivity hysteresis was revealed in the $(100 - x)$ $La_{0.6}Sr_{0.4}CoO_{3\pm\delta} - x\,CeO_2$ (LSCC) system over a wide concentration range (10 mol % $\leq x \leq$ 76 mol %).[18] It was shown that the shape of the hysteresis loop in the LSCC system depends upon the $La_{0.6}Sr_{0.4}CoO_{3\pm\delta}$ and $CeO_2$ ratio.[18] It does not depend on the heating/cooling rate (1−3 °C/min) and the types of electrodes used (Pt or Au). It is also reproducible on thermal cycling (50−900 °C). Such conductivity hysteresis was not observed in the $La_{0.8}Sr_{0.2}MnO_{3\pm\delta}$-$CeO_2$ and $La_{0.95}Ni_{0.6}Fe_{0.4}O_{3-\delta}$-$CeO_2$ systems.[18] It has been assumed so far that the appearance of the conductivity hysteresis in the LSCC system could be related to structural coherence at the phase interfaces between the rhombohedral structure of the modified perovskite and modified cubic fluorite structure of ceria. High temperature X-ray diffraction (XRD) carried out for a composite in the LSCC system showed the same evolution of the XRD patterns on heating and cooling, excluding the contribution of macro scale phase transformation in the origin of the hysteretic phenomenon.[18] However, structural and phase transformations at nano scale associated with oxygen release and oxygen accommodation cannot be ruled out. It was also noticed that the microstructure of composites in the LSCC system could play a certain role in the appearance of the conductivity hysteresis.[18] In the present study we explore the role of connectivity and interfacial interactions in determining transport properties of the 43 mol % $La_{0.6}Sr_{0.4}CoO_{3\pm\delta}$·57 mol % $CeO_2$ (LSCC57) composites. Phase equilibria in LSCC57 composites, crystal structure of constituents, surface composition, and electrical characteristics of the phase interface will be discussed as well. High resolution transmission electron microscopy has been applied to characterize phase composition at the nano scale. The LSCC57 composition was specially chosen for this investigation because it contains large fractions of both initial components and allows their characterization within the composite material with comparable accuracy.

## 2. Experimental Section

**2.1. Sample Preparation.** The initial perovskite $La_{0.6}Sr_{0.4}CoO_{3\pm\delta}$ (LSC) was produced by combustion spray pyrolysis and supplied by PRAXAIR Inc., U.S.A. $CeO_2$ delivered by ACROS ORGANICS (New Jersey, U.S.A.) was calcined at 1000 °C for 5 h to remove adsorbed water. The 43 mol % $La_{0.6}Sr_{0.4}CoO_{3\pm\delta}$·57 mol % $CeO_2$ (LSCC57) composites were fabricated by mixing of LSC and $CeO_2$ in the corresponding ratio in different ways: (i) in a mortar (LSCC57-M001); in a planetary ball mill (LSCC57-P008), and in a roller ball mill (LSCC57-R007, LSCC57-R048, LSCC57-R100 and LSCC57-R261). The three digits after "R", "P" and "M" stand for the total time of mixing and milling in hours. After the mixing followed by milling, all LSCC57 powders were fired in air at 1350 °C for 5 h. Specific surface area of LSC, $CeO_2$, and LSCC57 powders (as prepared and after calcination at 1350 °C) are presented in Table 1. In addition, $(100 - x)$ $La_{0.6}Sr_{0.4}CoO_{3\pm\delta}$·$x$ $CeO_2$ compositions (where $x$ = 2, 88, 89.4, and 92.4 mol %) were prepared by mixing of LSC and $CeO_2$ in mortar (for 1 h) and fired in air at 1350 °C for 5 h to study a solubility limit. For the sake of convenience, the abbreviations "LSCC system", LSCC57, LSCC2, LSCC88 and LSCC92.4 will be used further in the text for the description of the $(100 - x)$ LSC − $x$ $CeO_2$ system and the corresponding compositions. The three layered system LSC|$CeO_2$|LSC was fabricated through applying a $CeO_2$ slurry (0.001 g) to the top surface of a presintered LSC pellet (1350 °C). Two LSC pellets covered by $CeO_2$ slurry were joined together forming the three layered system, which was heated (1 °C/min) to 1350 °C under air and held for 5 h. The $CeO_2$ slurry was prepared through mixing of cerium oxide with polyethylene glycol (Sigma-Aldrich GmbH, Germany), dibutyle phtalate, poly(vinyl butyral), and ethyl methyl ketone (all three were provided by Fisher Scientific, U.K.), and ethanol (VWR international Ltd., U.K.). Preliminary investigation showed that all additional components of the slurry burn out in a temperature range up to 1000 °C.

**2.2. Characterization Methods.** Electrical conductivity of composite samples was measured on sintered pellets by the standard direct current (dc) four terminal method in a temperature range of 50−900 °C in static air at a heating/cooling rate of 0.6−3 °C/min. Au paste (T10112, Metalor Technologies Ltd., U.K.) was applied as current and potential probes.[19] To study an effect of oxygen partial pressure on conductivity of composites during heating and cooling stages, the electrical measurements were carried out in the same jig under nitrogen atmosphere (free from $O_2$) at 512 °C. The measurements were carried out in a narrow oxygen partial pressure range ($0.21 \leq a(O_2) \leq 1 \times 10^{-3}$ atm) since LSCC compositions are not stable in $H_2$−Ar atmosphere. The oxygen partial pressure in the chamber was monitored with an yttria-stabilized zirconia (YSZ) sensor. The signal monitored with the YSZ sensor showed linear variation on temperature in the range of 500−900 °C, thereby confirming the reliable reading for oxygen partial pressure at 512 °C. Electrochemical impedance spectroscopy (EIS) was carried out using a Hewlett-Packard 4192A LF impedance analyzer in the frequency range of 5 Hz−13 MHz and a system SI 1255 Frequency analyzer/SI 1287 Electrochemical interface in the frequency range of 0.01 Hz−100 kHz. The EIS measurements were taken under open circuit voltage (OCV) with the signal amplitude of 100 mV under static air. The data obtained were checked with a Kramers−Kronig validation program[20] and analyzed by the equivalent circuit method (through a non-linear least-squares fitting minimization procedure)[21] using the ZPlot electrochemical impedance software.[22] The equivalent circuit $(R_HQ_H)([R_{CT}Zw]Q_{INT})$ was applied to characterize the frequency response of the layered system, where $R_H$ is the high

(15) Stengel, M.; Vanderbilt, D.; Spaldin, N. A. *Nat. Mater.* **2009**, *8*, 392.
(16) Konisheva, E.; Gorbunova, E.; Neiman, A. Ya. *Solid State Ionics* **2001**, *141−142*, 141.
(17) Konysheva, E. Yu.; Neiman, A. Ya. *Russ. J. Electrochem.* **2002**, *38*, 369.
(18) (a) Konysheva, E.; Irvine, J. T. S. Abstracts of the 17th International Conference on Solid State Ionics, Alfred University: Toronto, Canada, June 28−July 3, 2009; p 11.; (b) Konysheva, E.; Irvine, J. T. S. *J. Phys. Chem. Chem. Phys*, submitted for publication.
(19) Konysheva, E.; Irvine, J. T. S. *J. Mater. Chem.* **2008**, *18*, 5147.
(20) Boukamp, B. A. *J. Electrochem. Soc.* **1995**, *142*, 1885.
(21) Boukamp, B. A. *Solid State Ionics* **1986**, *20*, 31.
(22) MacDonald, J. R. Zplot for Windows (Version 2.2) fitting program, LEVM 6.0.

**Table 1. Specific Surface Area of Powders, Relative Density of Pellets Characterized by Dilatometry, and Lattice Parameters of LSC, $CeO_2$, LSCC88, LSCC92.4, and Modified Constituents in LSCC57 Composites**

| | | | | modified perovskite ($R\bar{3}c$) | | | modified ceria, ($Fm\bar{3}m$) | |
|---|---|---|---|---|---|---|---|---|
| | | | | lattice parameters | | | | |
| | $S_{BET}$, $m^2/g$ (as prepared) | $S_{BET}$, $m^2/g$ after calcination at 1350 °C | relative density of pellets characterized by dilatometry | a [Å] | $\beta$ [deg] | volume, [Å]$^3$ | lattice parameter, a [Å] | volume, [Å]$^3$ |
| LSC | 7.60 ± 0.05 | 1.98 ± 0.09 | 92% | 5.4048(1) | 60.327(1) | 112.467(2) | | |
| LSCC57-P008 | 4.72 ± 0.07 | 0.37 ± 0.01 | 87% | 5.4088(1) | 60.339(2) | 112.749(4) | 5.4595(1) | 162.723(4) |
| LSCC57-M001 | 4.35 ± 0.02 | 0.77 ± 0.05 | 90% | 5.4110(1) | 60.351(1) | 112.916(9) | 5.4576(1) | 162.557(5) |
| LSCC57-R007 | 7.54 ± 0.10 | 2.45 ± 0.12 | 91% | 5.4122(2) | 60.341(3) | 112.966(8) | 5.4613(1) | 162.889(6) |
| LSCC57-R048 | 7.65 ± 0.04 | 0.40 ± 0.01 | 93% | 5.4200(3) | 60.341(4) | 113.456(10) | 5.4550(1) | 162.329(7) |
| LSCC57-R100 | 7.87 ± 0.08 | 0.78 ± 0.01 | | 5.4172(3) | 60.347(3) | 113.293(9) | 5.4554(1) | 162.362(7) |
| LSCC57-R261 | 13.06 ± 0.09 | 0.18 ± 0.01 | | 5.4173(3) | 60.335(4) | 113.270(9) | 5.4554(1) | 162.361(7) |
| LSCC88 | | | | | | | 5.4434(1) | 161.291(3) |
| LSCC92.4 | | | | | | | 5.4278(1) | 159.912(1) |
| $CeO_2$ | 2.34 ± 0.04 | | 86% | | | | 5.4103(9) | 158.37(5) |

frequency process; $R_{CT}$ is the charge-transfer resistance; $Q_H$ and $Q_{INT}$ are the constant phase elements for the high and low frequency processes, respectively; $Z_W$ is the finite length Warburg impedance (FLW)[23,24] characterizing oxygen diffusion. The impedance spectra were also analyzed with the equivalent circuit $(R_HQ_H)([R_{CT}Z_W]C_{DL})$, where $C_{DL}$ is an interfacial capacitance. However, better fitting parameters were obtained for the equivalent circuit $(R_HQ_H)([R_{CT}Z_W]Q_{INT})$. The constant phase element ($Q$) can be represented by the ratio $Y = Q(i\omega)^n$, where $Y$ is the admittance, "i" is the imaginary unit, "$\omega$" is the angular frequency, and "n" is the frequency power. The capacitances ($C_H$ and $C_{INT}$) were evaluated in accordance with the eq 1[25]

$$C_x = (R_x \times Q_x)^{1/n_x}/R_x \quad (1)$$

where $x$ is the corresponding index (H or INT), $n$ is the frequency power in the equation for the admittance, and $\pi$ has its usual meaning. The Warburg impedance was evaluated as following:[22]

$$Z_W = \frac{R_D \cdot \tanh \cdot ([i \cdot T \cdot \omega]^P)}{(i \cdot T \cdot \omega)^P} \quad (2)$$

where $R_D$ is the diffusion resistance; $T$ is expressed as $T = L^2/D$ ($L$ is an effective diffuse layer thickness and $D$ is an effective diffusion coefficient); and $P$ is a fractional exponent varying from 0 to 1.

Powder XRD data were recorded in air at room temperature in transmission mode on a Stoe Stadi-P diffractometer with Cu Kα radiation (Stoe & Cie GmbH, Germany). The diffraction spectra for all samples were registered in the angular range of $15 \le 2\Theta \le 96°$ with a step size of 0.1° and a recording time of 70 s for each step. Si powder (Alfa Aesar, Karlsruhe, Germany) was used as the external standard for the calibration of the diffractometer. The LSC|$CeO_2$ interface was characterized in reflection mode on a Philips analytical X-ray PW1710 diffractometer with Cu Kα radiation (Nederlandse Philips Bedrijven B.V., The Netherlands). The diffraction data were refined by the Rietveld method,[26] using the Generalized Structure Analysis System (GSAS) program.[27] The dilatometry investigation was carried out on a NETZSCH DIL 402C dilatometer (NETZSCH-Geraetebau GmbH, Germany) with a TASC 414/4 controller. LSCC57 pellets with a relative density of 86−93% (Table 1) were tested in air in a temperature range of 25−900 °C with a heating/cooling rate of 3 °C/min. Two thermal cycles were carried out for each sample. X-ray photoelectron spectroscopy (XPS) was applied to characterize the chemical state of elements. La 3d, Ce 3d, Co 2p, Sr 3d, O 1s, and C 1s core level spectra were recorded on powders with an ESCALAB II spectrometer (V.G., U.K.) using Al ($h\nu = 1486.4$ eV) radiation. Data were collected at a takeoff angle of 45°, allowing the characterization of the surface and the near surface region. A change in oxygen content in LSCC57 compositions during thermal cycling in air was studied by thermogravimetric analysis (TGA) on a NETZSCH TG 209 instrument (NETZSCH-Geraetebau GmbH, Germany). Measurements were carried out on powders in a temperature range of 25−900 °C at a heating/cooling rate of 3 °C/min. In addition, the samples were exposed to $H_2$−Ar (5% $H_2$−95% Ar) atmosphere in accordance with the approach described elsewhere[28] to characterize the average oxidation state of Co cations in the LSCC57 composites. The microstructural characterization of the sintered ceramic was carried out with a Jeol-JSM-5600 scanning electron microscope (SEM: JEOL, Tokyo, Japan) equipped with an energy dispersive X-ray (EDX) spectrometer of the Inca-energy 200 type (Oxford Instruments, Eynsham, U.K.). SEM images for all samples were taken on the polished surfaces as prepared without chemical or thermal etching. The SEM/EDX analysis allows quantitative analysis of large grains (~1 μm and

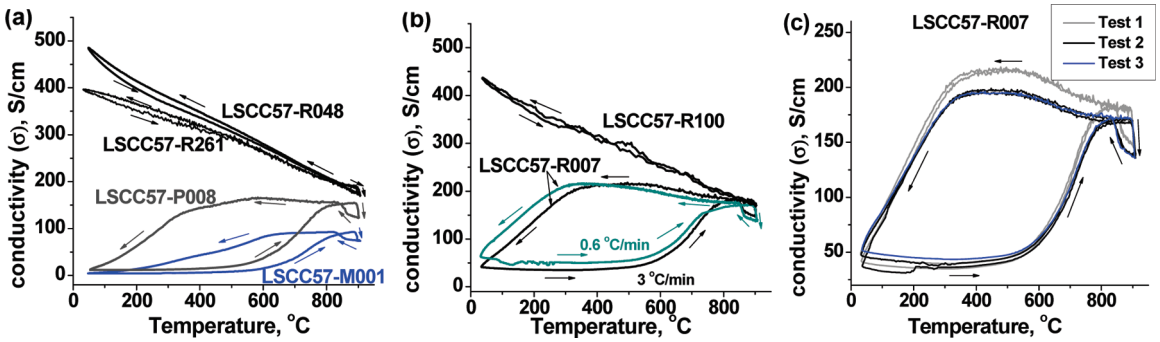


**Figure 1.** Electrical conductivity of LSCC57 composites; $a(O_2) = 0.21$, heating/cooling rate is 3 °C/min. Two-four thermal cycles were carried out for each sample. In addition, for LSCC57-R007 the thermocycle was carried out with a rate of 0.6 °C/min. The reversibility is demonstrated by the example of LSCC57-R007 (Figure 3c): 3 thermal cycles (Test 1) → the sample was taken out from the jig → 3 thermal cycles (Test 2) → the sample was taken out from the jig → 2 thermal cycles (Test 3).

larger). LSCC57 powders were also characterized by high-resolution transmission electron microscopy (HRTEM), transmission electron microscope Jeol JEM2011 (JEOL, Tokyo, Japan). The Brunauer−Emmett−Teller (BET) surface area, $S_{BET}$, was measured with $N_2$ on a TriStar II Instrument (Micrometrics Instrument Corporation, Norcross, U.S.A.). Laser Ablation Inductively Coupled Plasma Mass Spectrometry (LA-ICP-MS) was applied to analyze a chemical composition of LSCC57 samples fabricated in different ways (Agilent 7500a instrument, Agilent Technologies Ltd., U.K.).

## 3. Results and Discussion

**3.1. Conductivity of LSCC57 Composites.** The initial compounds $La_{0.6}Sr_{0.4}CoO_{3\pm\delta}$ (LSC) and $CeO_2$ possess different transport properties. LSC has high ionic conductivity ($\sigma_O = 0.22$ S/cm, at 800 °C in air) and high electronic conductivity (p-type, $\sigma_p = 1584$ S/cm at 800 °C in air).[29,30] LSC exhibits metallic conductivity in a wide temperature range. Conductivity of $CeO_2$ is lower by about 7 orders of magnitude at 800 °C than LSC.[31,32] The conductivity of LSCC2 (nearly single phase solid solution) decreases to ~921 S/cm at 800 °C because of the dissolution of cerium into the A-sublattice of the perovskite.[33] The conductivity of LSCC57-R048, LSCC57-R100, and LSCC57-R261 decreases to ~230 S/cm at 800 °C, which is higher by several orders of magnitude compared to $CeO_2$ and is lower by about a factor of 7 compared to LSC (Figure 1). These composites exhibit metallic-like behavior in the whole temperature range investigated, as for LSC, suggesting that the conductivities of LSCC57-R048, LSCC57-R100, and LSCC57-R261 are mainly determined by bulk and grain boundary conductivity of the modified perovskite constituent.

At room temperature the conductivity of LSCC57-R007, however, is distinctly lower compared to LSCC57-R048 (Figure 1). Moreover, conductivity hysteresis was observed for LSCC57-R007 in a temperature range of 50−800 °C independently of the heating/cooling rate (Figure 1b). The conductivity hysteresis was reversible on thermal cycling (Figure 1c). The conductivity of LSCC57-R007 is nearly constant on heating up to about 500 °C. The conductivity of LSCC57-R007 at this stage of thermal treatment is lower by about 3 orders of magnitude compared to LSC and it is higher by about 3 orders of magnitude compared to the ceria. The conductivity of LSCC57-R007 at this stage is too high to be related to the grain boundary or bulk conductivity of the modified ceria. This stage was assigned as an intermediate conductive state (ICS). After 600 °C a dramatic increase in the conductivity occurs. Metallic-like behavior becomes apparent after reaching 800 °C. Notice that LSCC57-R007 and LSCC57-R048 have comparable conductivity at high temperatures (800−900 °C). On cooling, the conductivity of LSCC57-R007 is higher by about a factor of 3 compared to that on heating and decreases drastically only after 300 °C. The conductivity of LSCC57-R007 on cooling to 300 °C was assigned as a high conductive state (HCS). Conductivity hysteresis was also observed for LSCC57-M001 and LSCC57-P008 (Figure 1a).

Figure 2 illustrates the effect of oxygen partial pressure on the conductivity of LSCC2, LSCC57-R048, and LSCC57-R007 at 512 °C in the coordinates "log $\sigma$" versus log $a(O_2)$. LSCC2 and LSCC57-R048 show p-type conductivity on heating at 512 °C. The p-type behavior in LSCC57-R007 within the ICS is almost suppressed (Figure 2). N-type conductivity becomes apparent in LSCC57-R007 with the lowering of the oxygen partial pressure ($\log a(O_2) < -1.5$), which is typical of $CeO_2$.[31,32] After heating to 900 °C in air followed by cooling to 512 °C (HCS), LSCC57-R007 exhibits only the p-type conductivity through the whole $a(O_2)$ range investigated.

The presence of the modified ceria as an addition phase could influence the electronic conductivity in LSCC composites. According to the literature,[31,32] oxygen vacancies and electrons are the dominant charge carriers in $CeO_2$. In this case, the recombination of electrons (from the

(23) Boukamp, B. A., *Equivalent Circuit User's Manual*; University of Twente: Twente, The Netherlands, 1989.
(24) Macdonald, J. R. *Impedance Spectroscopy. Emphasizing Solid Materials & Systems*; John Wiley & Sons: New York, 1987; p 60.
(25) Fleig, J. *Solid State Ionics*. **2002**, *150*, 181.
(26) Rietveld, H. M. *J. Appl. Crystallogr*. **1969**, *2*, 65.
(27) Larson, A. C.; von Dreele, R. B. *GSAS - Generalized Structure Analysis System*; Los Alamos National Laboratory Report LAUR-86-748; Los Alamos National Laboratory: Los Alamos, NM, 1994.
(28) Konysheva, E.; Irvine, J. T. S. *Chem. Mater*. **2009**, *21*, 1514.
(29) Teraoka, Y.; Zhang, H. M.; Okamoto, K.; Yamazoe, N. *Mater. Res. Bull*. **1998**, *23*, 51.
(30) Ullmann, H.; Trofimenko, N.; Tietz, F.; Stover, D.; Ahmad-Khanlou, A. *Solid State Ionics* **2000**, *138*, 79.
(31) Tuller, H. L.; Nowick, A. S. *J. Electrochem. Soc*. **1979**, *126*, 209.
(32) Tschope, A.; Sommer, E.; Birringer, R. *Solid State Ionics* **2001**, *139*, 255.
(33) Konysheva, E.; Francis, S. M.; Irvine, J. T. S. *J. Electrochem. Soc*. **2010**, *157*, B159.

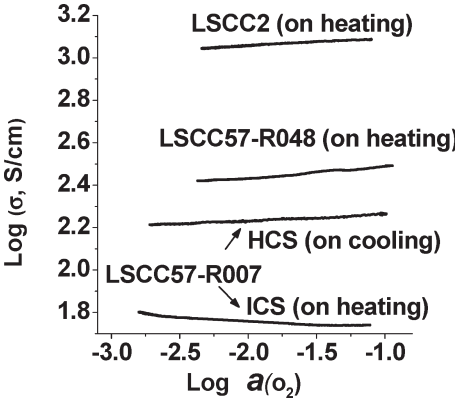


**Figure 2.** Conductivity of LSCC2, LSCC57-R048 and LSCC57-R007 during exposure to nitrogen atmosphere (free from $O_2$) at 512 °C; the reduction stage.

modified ceria) and holes (from the modified perovskite) could occur at 2D or 1D interfaces between the constituents in LSCC57-R048, LSCC57-R100, and LSCC57-R261, resulting in the depletion of charge carriers at phase interfaces and suppressing the electronic conductivity. This could take place even if charge transfer pathways do not cross the phase interfaces.

**3.2. Phase Composition and Crystal Structure of LSCC57 Composites.** At room temperature $La_{0.6}Sr_{0.4}CoO_{3\pm\delta}$ (LSC) exhibits rhombohedrally distorted perovskite structure, space group $R\bar{3}c$ (no. 167), whereas $CeO_2$ displays a fluorite structure, space group $Fm\bar{3}m$ (no. 225).[34,35] According to XRD all LSCC57 compositions are two phase at room temperature (Figure 3). They are composed of the modified perovskite with rhombohedral structure ($R\bar{3}c$, no. 167) and modified ceria with fluorite structure ($Fm\bar{3}m$, no. 225). A broadening of the diffraction peaks was observed in the XRD patterns of LSCC57-R048, LSCC57-R100, and LSCC57-R261. The diffraction peaks in the XRD patterns of LSCC57-M001, LSCC57-P008, and LSCC57-R007 are sharp. One can clearly distinguish peaks related to different phases. A low amount of cerium (~2 mol %) can dissolve in the perovskite structure.[33,36] $La_2O_3$, SrO, and Co containing oxides can individually dissolve in the fluorite structure of $CeO_2$.[37−41] The double doping effect was also reported for the $(Ce_{1-x-y}La_xM_y)O_{2-\delta}$ (M = Ca, Sr) system.[42] LSCC98, LSCC92.4, and LSCC88 are single phase solid solutions with the cubic symmetry ($Fm\bar{3}m$, no. 225) (Table 1), demonstrating that La, Sr, and Co cations can dissolve simultaneously in the fluorite structure. SEM/EDX analysis carried

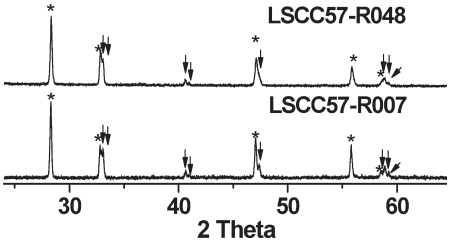


**Figure 3.** XRD patterns of LSCC57-R007 and LSCC57-R048 composites after firing at 1350 °C for 5 h in air. XRD patterns were recorded at room temperature in the transmission mode. The diffraction peaks related to a phase with rhombohedral perovskite structure, $R\bar{3}c$, (*) and a phase with fluorite structure, $Fm\bar{3}m$, (↓) are marked on the figure.

out on large particles in LSCC57 compositions confirmed the cross-dissolution of cations between the parent LSC and $CeO_2$. For instance, the particles of the modified perovskite in LSCC57-P008 contain 1−7 at. % Ce and the modified ceria particles contain 10−17 at. % La, 1−4 at. % Sr, and 1−6 at. % Co.

The incorporation of lanthanum or strontium into the fluorite structure of $CeO_2$ should be accompanied by an increase in the lattice parameter.[37−39] A decrease in the lattice parameter of Co modified ceria might be expected because of the difference in the ionic radii: $r^{VIII}_{Ce^{4+}} = 0.97$ Å; $r^{VI}_{Co^{2+}(HS)} = 0.735$ Å, and $r^{VI}_{Co^{3+}(HS)} = 0.61$ Å;[43] however, because of decrease in oxygen content it is more likely that the unit cell will expand. Although it would be difficult to reveal by XRD if La, Sr, and Co cations dissolve simultaneously in the fluorite structure. The lattice parameters of the modified ceria in all LSCC57 compositions are much higher compared to those for the single phase LSCC92.4 and $CeO_2$ as an individual phase (Table 1), but they are closer to that for the single phase LSCC88. The lattice parameters of the modified perovskite are slightly higher compared to LSC (Table 1), and they are close to those reported for LSCC2 nearly single phase solid solution: $a = 5.4118$ Å and $\beta = 60.349°$, $V = 112.959$ Å$^3$ (data were converted from the hexagonal setting).[33] However, the lattice parameters of both constituent in all LSCC57 compositions are slightly different (Table 1), implying that the fabrication procedure slightly influence the structural parameters of the constituents in the LSCC57 composites. The modified perovskite in LSCC57-M001, LSCC57-P008, and LSCC57-R007 (which show the conductivity hysteresis) has slightly smaller lattice parameters and cell volume compared to that in LSCC57-R048, LSCC57-R100, and LSCC57-R261 (which do not exhibit the conductivity hysteresis). In contrast, the modified ceria in LSCC57-M001, LSCC57-P008, and LSCC57-R007 has slightly larger lattice parameter and cell volume compared to LSCC57-R048, LSCC57-R100, and LSCC57-R261. This could alter the local structure of the anionic sublattices of the modified perovskite and modified ceria. It is particularly important because both parent LSC and $CeO_2$ possess significant ionic conductivity. A closer inspection of O−O distances obtained from the refinement of the XRD patterns recorded in the transmission mode indicates the

(34) Sonntag, R.; Neov, S.; Kozhukharov, V.; Neov, D.; ten Elshof, J. E. *Physica B* **1998**, *241−243*, 39.
(35) Varez, A.; Garcia-Gonzalez, E.; Jolly, J.; Sanz, J. *J.Eur. Ceram. Soc.* **2007**, *27*, 3677.
(36) Wen, Y.; Zhang, C.; He, H.; Yu, Y.; Teraoka, Y. *Catal. Today* **2007**, *126*, 400.
(37) Morris, B. C.; Flavell, W. R.; Mackrodt, W. C.; Morris, M. A. *J. Mater. Chem.* **1993**, *3*, 1007.
(38) Dikmen, S.; Shuk, P.; Greenblatt, M. *Solid State Ionics* **1999**, *126*, 89.
(39) Chavan, S. V.; Tyagi, A. K. *Thermochim. Acta* **2002**, *390*, 79.
(40) Zhang, T.; Hing, P.; Huang, H.; Kilner, J. *J. Eur. Ceram. Soc.* **2002**, *22*, 27.
(41) Chen, M.; Hallstedt, B.; Grundy, A. N.; Gauckler, L. J. *J. Am. Ceram. Soc.* **2003**, *86*, 1567.
(42) Yamamura, H.; Katoh, E.; Ichikawa, M.; Kakinuma, K.; Mori, T.; Haneda, H. *Electrochemistry* **2000**, *68*, 455.
(43) Shannon, R. D.; Rewitt, C. T. *Acta Crystallogr., Sect. B* **1969**, *25*, 925.

possible epitaxial coherence between oxygen sublattices of the constituents in the LSCC57 composites (Figure 4). However, in LSCC57-M001, LSCC57-P008, and LSCC57-R007, which show the conductivity hysteresis, the difference between one set of O−O distances in the modified perovskite and O−O distances in the modified ceria exceeds slightly 0.005 Å (Figure 4) and is larger than for LSCC57-R048, LSCC57-R100, and LSCC57-R261 that do not show such significant hysteresis.

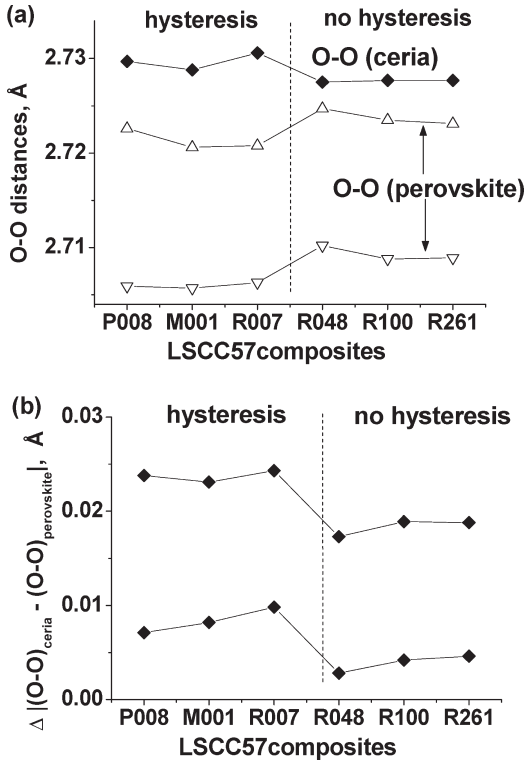


**Figure 4.** (a) O−O distances in the modified perovskite and modified ceria; (b) the difference between O−O distances in the modified perovskite and modified ceria. Data obtained from the refinement of the XRD data recorded at room temperature in transmission mode.

**3.3. Chemical and Structural Transformations with Temperature Variation.** Dilatometry and thermogravimetric analysis (TGA) can provide information on structural and chemical changes occurring in the volume of LSCC57 composites with temperature variation (Figures 5 and 6). The values of the thermal expansion coefficients (TEC) are presented in Table 2. The thermal expansion of LSC is higher than $CeO_2$, in particular, in the temperature range of 600−900 °C (Figure 5a and Table 2). A strong change in TEC of the parent LSC occurs most probably because of the symmetry transformation $R\bar{3}c \rightarrow Fm\bar{3}m$, which is accompanied by oxygen loss and increase in the concentration of oxygen vacancies.[34] One can distinguish two regions with different TEC for all LSCC57 composites investigated (Figure 5 and Table 2). On heating and cooling the same values of TEC were observed for LSCC57-P008, LSCC57-R007, and LSCC57-R048, although those for LSCC57-M001 were slightly different. Slight variations in TEC of the LSCC57 composites fabricated in different ways were observed because of the linear thermal expansion of composite materials includes contributions not only from thermal expansion of the crystal lattices of individual components (the modified ceria and modified perovskite), but also variations in microstructure of the composites (the particle sizes of both constituents and their distribution through the volume). There is no correlation between TEC variations and whatever hysteresis was observed.

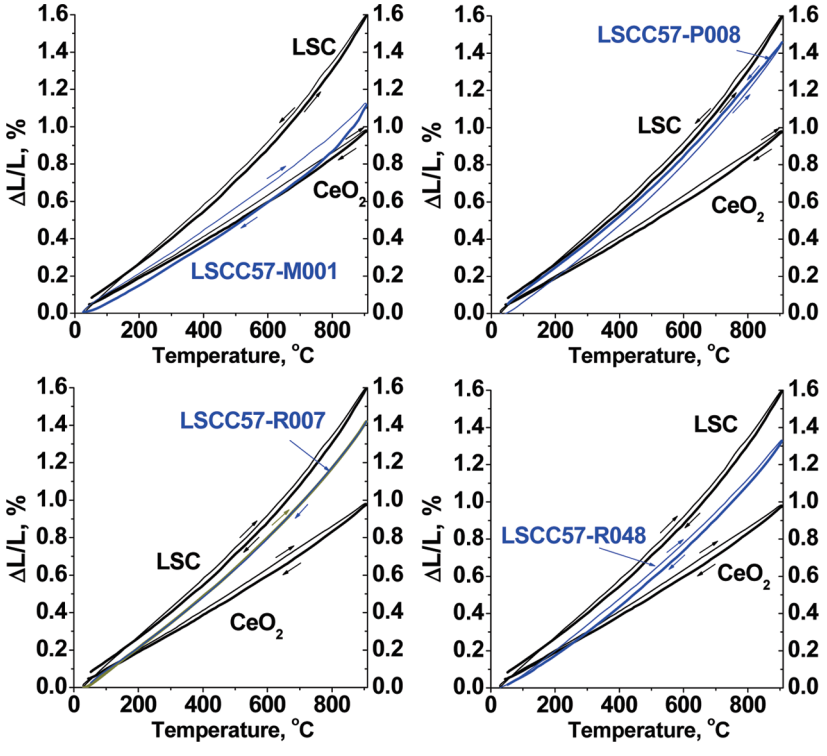


**Figure 5.** Thermal expansion of LSCC57-M001, LSC57-P008; LSCC57-R007, and LSCC57-R048 in comparison with the parent LSC and $CeO_2$.

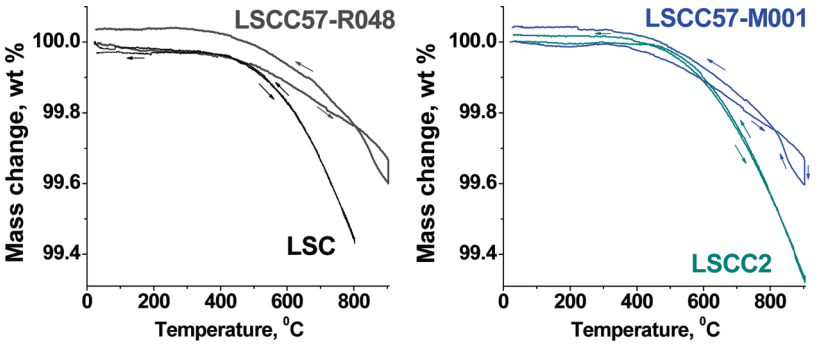


**Figure 6.** Thermogravimetric analysis of LSCC57-R048 and LSCC57-M001 compared to LSC and LSCC2 in air on powders; heating/cooling rate is 3 °C/min.

**Table 2. Thermal Expansion Coefficients of LSCC57 Composites Compared to LSC and $CeO_2$**

| composition | regime | thermal expansion coefficient | |
|---|---|---|---|
| LSC | cooling down | $15.3 \times 10^{-6}$ $K^{-1}$ (200−600 °C) | $23.3 \times 10^{-6}$ $K^{-1}$ (600−900 °C) |
| LSCC57-M001 | heating up | $11.6 \times 10^{-6}$ $K^{-1}$ (200−700 °C) | $15.4 \times 10^{-6}$ $K^{-1}$ (700−900 °C) |
| | cooling down | $11.3 \times 10^{-6}$ $K^{-1}$ (200−700 °C) | $18.3 \times 10^{-6}$ $K^{-1}$ (700−900 °C) |
| LSCC57-P008 | cooling down | $14.9 \times 10^{-6}$ $K^{-1}$ (200−600 °C) | $19.9 \times 10^{-6}$ $K^{-1}$ (600−900 °C) |
| LSCC57-R007 | cooling down | $14.6 \times 10^{-6}$ $K^{-1}$ (200−600 °C) | $20.3 \times 10^{-6}$ $K^{-1}$ (600−900 °C) |
| LSCC57-R048 | cooling down | $14.1 \times 10^{-6}$ $K^{-1}$ (200−600 °C) | $19.2 \times 10^{-6}$ $K^{-1}$ (600−900 °C) |
| $CeO_2$ | cooling down | $11.1 \times 10^{-6}$ $K^{-1}$ (200−900 °C) | |

All LSCC57 compositions show the same weight change in TGA experiments (Figure 6). Oxygen release is slightly suppressed in LSCC57 composites with increasing temperature compared to the oxygen accommodation, which could be caused by the presence of the modified ceria as a secondary phase at the interface. The oxygen loss during the reduction of LSCC57-M001 and LSCC57-R048 in $H_2$−Ar atmosphere was similar: $-6.45 \pm 0.08$ wt % and $-6.43 \pm 0.01$ wt %, respectively, indicating the same average values of the oxidation state of Co cations in the LSCC57 composites.

Data presented in this section demonstrate that on heating and cooling similar processes occur in the volume of all LSCC57 composites, irrespectively of processing conditions.

**3.4. Chemical State and Surface Composition at Room Temperature.** X-ray Photoelectron Spectroscopy (XPS) was used to study the chemical states of Co, La, Ce, Sr, and O in LSCC57-M001, LSCC57-P008, LSCC57-R048, and LSCC57-R261. The La $3d_{5/2}$, Co $2p_{3/2}$, and O 1s core level spectra were compared to those for LSC (Figure 7). Surface compositions of the samples derived from XPS measurements are presented in Table 3, and compared to the volume stoichiometry of the LSCC57. The chemical state of La in LSCC57-M001 and LSCC57-P008 is similar to that in LSC. The La $3d_{5/2}$ spectra of LSCC57-R048 and LSCC57-R261 shifted toward lower binding energy. In contrast to LSCC57-M001 and LSCC57-P008, the surface concentration of La in LSCC57-R048 and LSCC57-R261 is lower (Table 3), indicating the dissolution of lanthanum in the bulk of the modified phases. The La $3d_{5/2}$ spectra of all LSCC57 have nearly the same full width at half minimum as for LSC. A slight enrichment of the surface by strontium was revealed for all samples, which is typical of Co and Mn containing perovskites.[44,45] The Ce concentration on the surface is less compared to the theoretical value for all LSCC57 samples (Table 3).

According to XPS, the chemical state of Co is nearly the same in all LSCC57 composites, which correlates with the results of TGA (Figure 6), and similar to that in LSC (Figure 7). Only for LSCC57-P008, Co $2p_{3/2}$ spectra shifted slightly toward low binding energy ($\Delta E_B = 0.4$ eV), which is a little larger shift than the accuracy of the XPS measurement (~0.1−0.2 eV). However, the Co $2p_{3/2}$ spectra of all LSCC57 are broader compared to LSC (Figure 7), indicating the involvement of Co cations in local disorder taking place at the surface or near surface area. The Co concentration on the surface of all samples is less by about a factor of 2 compared to the volume ratio (Table 3). It might be interpreted as a redistribution of Co cations between the surface and the bulk of crystallites. On the other hand, the low value of the Co concentration on the surface of all samples might indicate that the Co cations are the preferable surface sites for the oxygen sorption. Notice that the surface of all samples is enriched by oxygen, in particular, for LSCC57-R048 (Table 3).

O 1s spectra recorded for LSCC57 compositions are complex, as for the parent LSC. In contrast to LSC, however, the peaks in the O 1s spectra of LSCC57 composites are broader, like for Co 2p spectra, and they are shifted toward high binding energy (Figure 7). In addition, there is a slight difference in the O 1s spectra recorded for LSCC57 composites. In composites, which do not show conductivity hysteresis, the peaks at a lower binding energy $E_B \sim 528.4$ eV (LSCC57-048) and $E_B \sim 528.5$ eV (LSCC57-R261) can be assigned to the lattice oxygen, as for LSC ($E_B \sim 528.2$ eV).[44,46,47] It might be interpreted as

(44) van der Heide, P. A. W. *Surf. Interface Anal.* **2002**, *33*, 414.
(45) Konysheva, E.; Irvine, J. T. S.; Besmehn, A. *Solid State Ionics* **2009**, *180*, 778.
(46) Database for Surface Spectroscopy http://www.lasurface.com (accessed November 2009).
(47) Wang, P.; Yao, L.; Wang, M.; Wu, W. *J. Alloys Compd.* **2000**, *311*, 53.

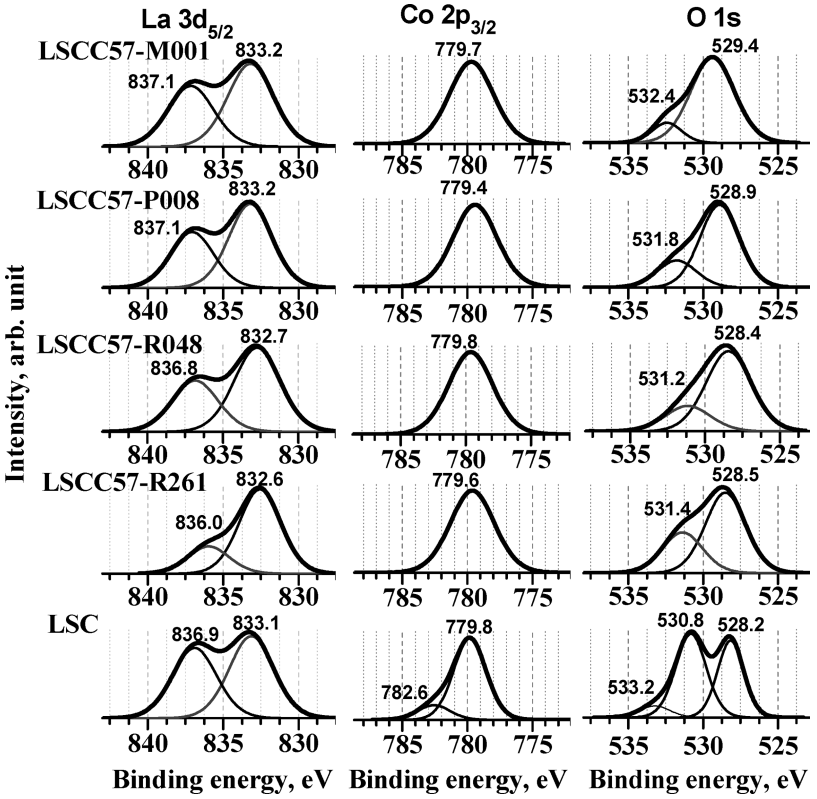


**Figure 7.** La $3d_{5/2}$, Co 2 $p_{3/2}$, and O 1s core level spectra of LSC, LSCC57-M001, LSCC57-P008, LSCC57-R100, and LSCC57-R261. The accuracy of the XPS measurements is ~0.2−0.1 eV.

**Table 3. XPS-Derived Compositions of LSCC57 Composites**

| | at., % | | | | |
|---|---|---|---|---|---|
| element | volume[a] | LSCC57-M001 | LSCC57-P008 | LSCC57-R048 | LSCC57-R261 |
| La | 6.7 | 5.9 | 5.0 | 4.0 | 2.0 |
| Sr | 4.4 | 5.6 | 7.0 | 5.3 | 6.8 |
| Co | 11.1 | 6.1 | 4.9 | 3.4 | 5.5 |
| O | 63 | 74.2 | 73.9 | 81.4 | 74.8 |
| Ce | 14.8 | 8.2 | 9.2 | 5.9 | 10.9 |

[a] Volume stoichiometry of the LSCC57 composition.

similar mobility of the lattice oxygen in LSC, LSCC57-R048, and LSCC57-R261, indicating an absence of obstructions for oxygen transport in the area directly adjusted to the phase interfaces and across the interface {modified perovskite/modified ceria}. Notice that the smallest difference in the O−O distances in the modified perovskite and modified ceria was revealed for LSCC57R-048, LSCC57-R100, and LSCC57-R261 (Figure 4). The peaks at higher binding energy $E_B \sim 531.2$ eV (LSCC57-R048) and $E_B \sim 531.4$ eV (LSCC57-R261) could be attributed to the surface states: Co−O species in perovskites[44] as well as cerium and cobalt hydroxides.[48] In the case of LSCC57-M001 and LSCC57-P008, which exhibit conductivity hysteresis, O 1s spectra shifted much stronger toward high binding energy. The peak at lower binding energy $E_B \sim 528.9$ eV in the O 1s spectrum of LSCC57-P008 could be also assigned to the lattice oxygen in the perovskite structure. However, a shift by about 0.7 eV could indicate a noticeable change in the local environment of oxygen ions in the near surface area. The peak at higher binding energy ($E_B \sim 531.8$ eV) could be attributed to $CO_3^{2-}$ surface species.[44] On the other hand, the appearance of the peak at $E_B \sim 531.7-531.8$ eV in the O 1s spectrum was reported for Co foil oxidized under oxygen atmosphere at 200 and 400 °C,[49] which may be interpreted as an existence of a certain fraction of $Co^{2+}$ cations at the surface. It seems to be reasonable because the strongest shift of the peak to a low binding energy ($\Delta E_B = 0.4$ eV) among the samples investigated was revealed in the Co $2p_{3/2}$ spectrum of LSCC57-P008 (Figure 7). For LSCC57-M001, the peak at lower binding energy ($E_B \sim 529.4$ eV) can be assigned to Sr−O surface species in perovskite[44] and to Ce in mixed oxides.[50] Close values of the binding energy for structural elements related to crystal lattices of different phases might lead to an interaction between the modified perovskite constituent and modified ceria in LSCC57-M001 composite not only through oxygen sublattices, but also through the cation sublattice of the modified perovskite and oxygen sublattice of the modified ceria. The peak at higher binding energy ($E_B \sim 532.4$ eV) in the O 1s spectrum of LSCC57-M001 is difficult to assign. The binding energy is high to be ascribed to $CO_3^{2-}$ surface species ($E_B \sim 531.6-532.0$ eV) and it is low to be assigned to chemisorbed dioxygen species ($E_B \sim 532.7-533.5$ eV).[44]

To conclude, the surface concentration of La is lower and La−O bonds have lower binding energy in

(48) Barr, T. L. *J. Phys. Chem.* **1978**, *82*, 1801.

(49) Galtayries, A.; Grimblot, J. *J. Electron Spectrosc. Relat. Phenom.* **1999**, *98−99*, 267.

(50) Galtayries, A.; Blanchard, G.; Riga, J.; Caudano, R.; Sporken, R. *J. Electron Spectrosc. Relat. Phenom.* **1998**, *88−91*, 951.

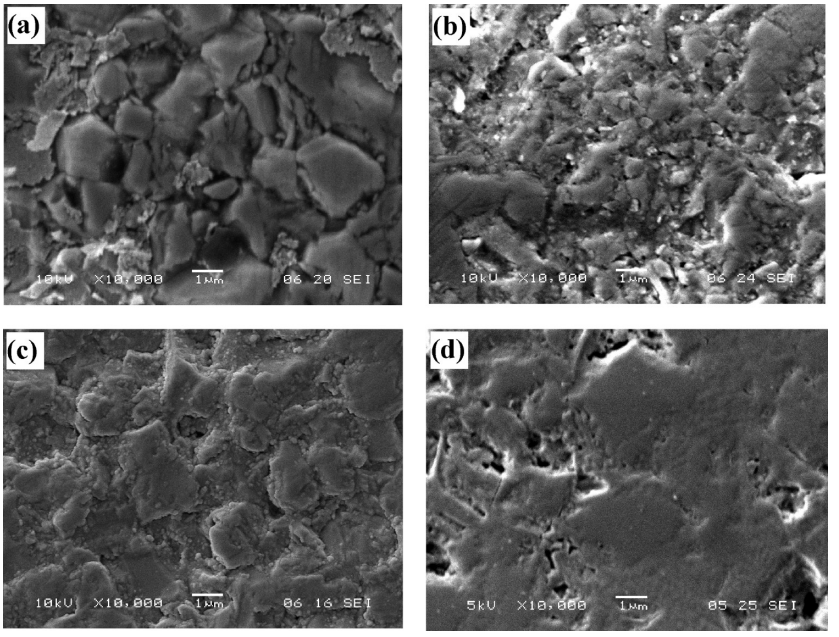


**Figure 8.** SEM images of materials sintered at 1350 °C: (a) LSCC57-P008, (b) LSCC57-R007, (c) LSCC57-R048, and (d) LSCC57-R261.

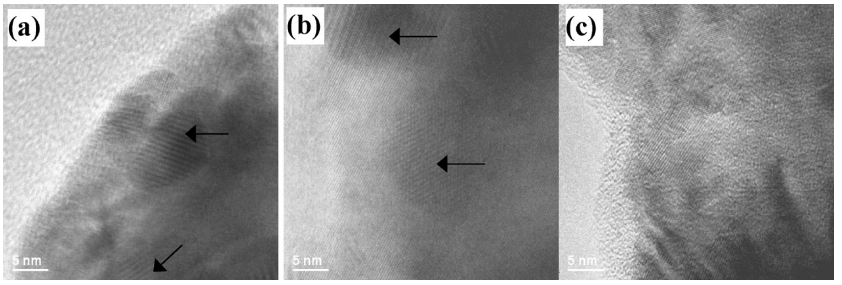


**Figure 9.** TEM images: (a)-(b) single crystal particles in LSCC57-R007 and LSCC57-P008; areas on the surface of these particles with large *d*-spacings are marked by arrows; (c) polycrystalline particle covered by amorphous layer in LSCC57-R048.

LSCC57-R048 and LSCC57-R261 in contrast to LSCC57-M001 and LSCC57-P008. Both surface oxygen states and lattice oxygen in the area directly adjusted to the surface have stronger binding energy in LSCC57-M001 and LSCC57-P008 composites showing conductivity hysteresis.

**3.5. Microstructure Characterization of LSCC57 Composites.** SEM was used to characterize the microstructure of LSCC57 pellets, whereas powders from the same batch as the pellets were examined by HRTEM. The results are presented in Figures 8 and 9, considering first LSCC57-P008 and LSCC57-R007, which show strong conductivity hysteresis on thermal cycling.

The size of grains in LSCC57-P008 varies from 0.5 $\mu$m up to several micrometers for both modified perovskite and modified ceria (Figure 8a). In LSCC57-R007, the grains of both modified phases are smaller in size (Figure 8b). They are randomly distributed through the volume of LSCC57-P008 and LSCC57-R007. In contrast to LSCC57-R048 and LSCC57-R261, the grains of the modified perovskite in LSCC57-P008 and LSCC57-R007 do not form a continuous medium: these grains do not have good contact between each other, or the network of the modified perovskite grains is interrupted by grains of the modified ceria (Figure 8a and b). TEM investigation showed even more noticeable difference between LSCC57-P008/LSCC57-R007 and LSCC57-R048/LSCC57-R261 powders. According to TEM, LSCC57-P008 powder composes single crystal particles only. The single crystal particles were covered by an amorphous layer. In LSCC57-R007 beside the single crystal particles, few very small polycrystalline particles were observed, but they were unstable even under weak electron beam. However, areas with much larger *d*-spacing (4.0 Å, 4.4 Å, 5.6 Å, 6.6 Å, 1.01 Å and 3.1, 4.6, 9.4 Å) were regularly observed on the surface of single crystal particles in both LSCC57-P008 and LSCC57-R007 (Figure 9a and b), which could be formally related to $Ce_{11}O_{20}$ phase (JCPDS 089−8435, triclinic structure)[51] and $La_4Co_3O_{10}$ (JCPDS 070−2680, monoclinic symmetry).[51] Nanoscale phase transformations occurring at the interface between the modified perovskite and modified ceria in LSCC57-P008 and LSCC57-R007 could be presented schematically by the following reactions

$$(LaSrCe)CoO_3 + (CeLaSrCo)O_{2-\delta} \rightarrow (CeLaSrCo)_{11}O_{20} + La_4Co_3O_{10} \quad (3)$$

(51) International Centre for Diffraction Data, Database PDF-2 (accessed October 2009).

It is less likely that two-dimensional rearrangements on the interface with the involvement of limited number of atoms could be limited by kinetics. The family of cerium oxides with different oxygen content is wide,[52,53] but oxygen partial pressure below $\sim 10^{-8}$ atm is required to introduced oxygen deficiency in undoped $CeO_2$.[54] However, oxygen deficiency in cerium oxides could be introduced through doping by cations with lower oxidation state. The presence of $Ce_6O_{11}$ was revealed by XRD in $La_{0.6}Ce_{0.4}CoO_3$ calcined in air at 700 °C.[55] $(LaCe)_{11}O_{20}$ was discovered in the 25 mol % $CeO_2$-75 mol % $La_{0.95}Ni_{0.6}Fe_{0.4}O_3$ composition fired in air at 1350 °C.[18] High oxygen deficiency could be introduced within cerium oxides ($Ce^{4+}$, $r^{VIII}_{Ce^{4+}} = 0.97$ Å)[40] even under air through multidoping with Sr ($r^{VIII}_{Sr^{2+}} = 1.25$ Å),[43] Co ($r^{VI}_{Co^{2+}(HS)} = 0.735$ Å),[43] and La ($r^{VIII}_{La^{3+}} = 1.18$ Å).[43] Noticeable difference in the radii of the matrix cation and dopants could lead to strong distortions of the crystal lattice of the modified ceria, finally resulting in the appearance of a phase with lower symmetry.

Further we discuss the microstructure of the LSCC57-R048 and LSCC57-R261 composites that do not show hysteresis (Figure 8c and d). The average size of the modified perovskite grains in LSCC57-R048 is about 2−4 $\mu$m. They are well connected with each other (Figure 8c), forming a continuous network through the composite material. One can also see a very good two-dimensional connectivity between perovskite grains in LSCC57-R261 (Figure 8d). The modified perovskite grains are surrounded by Ce-containing small particles with the average size of 100−300 nm (Figure 8c) or Ce-containing small particles are situated inside of pores (Figure 8d), which are out of charge and mass transfer pathways. According to TEM, both LSCC57-R048 and LSCC57-R261 powders consist of single crystal particles and polycrystalline particles. The polycrystalline particles were also covered by an amorphous layer with a thickness of about 5 nm (Figure 9c). However, a large amorphous region, containing nanosize $CeO_2$ particles (defined from the *d*-spacings) embedded by amorphous phase, was also observed. TEM/EDX indicates the presence of all four elements (La, Sr, Ce, and Co) in the amorphous phase. The polycrystalline particles in LSCC57-R048 and LSCC57-R261 consist of randomly orientated one-dimensional and two-dimensional structures with different *d*-spacings. The *d*-spacings defined from diffraction patterns could be attributed to Ce, La, and Sr containing phases: $CeO_2$ (JCPDS 044-1001, hexagonal symmetry),[51] $SrCeO_3$ (JCPDS 036-0980, orthorhombic structure),[51] $La_4SrO_7$ (JCPDS 022-1430, hexagonal structure),[51] $Sr_2CeO_4$ (JCPDS 022-1422, hexagonal structure),[51] $SrCeO_3$ (JCPDS 036-0980, orthorhombic structure),[51] and $La_4Sr_3O_9$ (JCPDS 072-0893, monoclinic structure).[51] This gives additional evidence on the exsolution of La and Sr from the volume of the modified perovskite phase and their involvement in a wide variety of phase and structural transformations at the nano scale.

One can see that the composites that show conductivity hysteresis do not have good connectivity between the grains of the modified perovskites through the bulk of the materials. These composites are preferably composed single crystal particles. Nanoscale phase transformations occurring at the surface of single crystal particles in powders, which would be interfaces in the sintered composites, demonstrate interesting and important differences from those which were observed in the composites that do not show conductivity hysteresis.

**3.6. Role of Phase Interfaces and Chemical Interaction on Phase Interfaces in Transport Properties of LSCC Composites.** Composites with different fabrication history show different conduction behavior on thermal cycling (Figure 1). Below 800 °C LSCC57-R007, LSCC57-M001, and LSCC57-P008 exhibit strong reversible conductivity hysteresis on heating (intermediate conductive state, ICS) and cooling (high conductive state, HCS) independently of the heating/cooling rate (Figure 1). In the ICS, the value of the conductivity is lower by about 3 orders of magnitude compared to LSC, but it is too high to be related to bulk or grain boundary conductivity of $CeO_2$. The p-type electronic conductivity in LSCC57-R007 is barely evident in the ICS compared to that in the HCS and compared to those in LSCC2 and LSCC57-R048 (Figure 2).

Similar structural and chemical changes occur in the volume of all LSCC57 composites on heating and cooling stages: (i) similar values of thermal expansion coefficient were observed for all LSCC57 (Figure 5) and (ii) the same phase evolution was observed in LSCC57-M001.[18] Slight hysteresis was observed during oxygen desorption and accommodation in all composites, but it is within 0.2 wt % only (Figure 6). Because of preferable dissolution of La, Sr, and Co from LSC into the fluorite structure of ceria, epitaxial coherence between oxygen sublattices at phase interfaces in all LSCC57 composites becomes apparent, thereby strongly changing the lattice parameters of the fluorite structure and, in particular, the oxygen sublattice. At macro scale, however, in the composites that exhibit conductivity hysteresis the difference between one set of O−O distances in the modified perovskite and O−O distances in the modified ceria is slightly larger (Figure 4). Both lattice oxygen and surface oxygen states have stronger binding energy (Figure 7). The surface concentration of La is higher (Table 2). Nanoscale transformations taking place at the interface between the modified perovskite and modified ceria are also different, eq 3. Another important result is that the modified perovskite grains in the composites, which show conductivity hysteresis, do not form a continuous network (Figure 8a and b). Charge and mass transfer pathways in this case could cross the chemically modified phase interfaces and result in more complex behavior with temperature variation.

In contrast, LSCC57-R048 and LSCC57-R261, which do not show conductivity hysteresis, have good connectivity between the modified perovskite grains (Figure 8c and d),

(52) Eyring, L. *Synthesis of Lanthanide and Actinide Compound*; Kluwer Academic Publisher: The Netherlands, 1991; p 187.
(53) Zinkevich, M.; Djurovic, D.; Aldinger, F. *Solid State Ionics* **2006**, *177*, 989.
(54) Hull, S.; Norberg, S. T.; Ahmed, I.; Eriksson, S. G.; Marrocchelli, D.; Madden, P. A. *J. Solid State Chem.* **2009**, *182*, 2815.
(55) Wen, Y.; Zhang, C.; He, H.; Yu, Y.; Teraoka, Y. *Catal. Today* **2007**, *126*, 400.

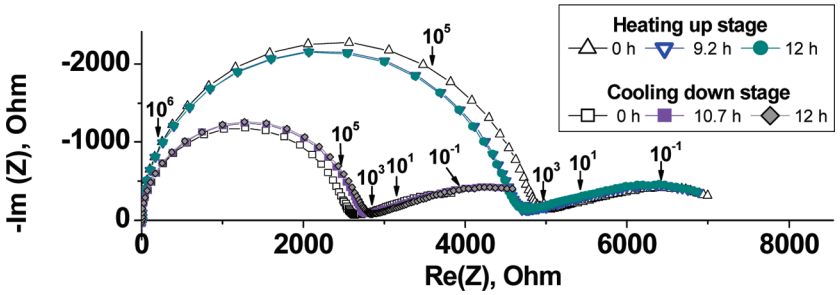


**Figure 10.** Impedance spectra of the LSC|$CeO_2$|LSC three layered system recorded at 500 °C on heating (ICS) and cooling (HCS); $a(O_2) = 0.21$.

indicating that their conductivity is mainly determined by bulk and intergrain conductivities of the modified perovskite phase. Similar values of the binding energy for the lattice oxygen in these composites and LSC (Figure 7) could imply comparable mobility of lattice oxygen and an absence of obstructions for oxygen transport at near surface area and across the interface {modified perovskite/modified ceria}.

These observations suggest that the origin of the conductivity hysteresis could be related to the chemically modified interface LSC/$CeO_2$ or co-doped $CeO_2$ as there are no clear alternative explanations. The well-defined LSC|$CeO_2$|LSC three layered model system was investigated to explore the role of phase interfaces in more detail.

**3.7. Three Layered Model Interface LSC|$CeO_2$|LSC: Transport Properties, Phase and Chemical Composition.** The three layered system LSC|$CeO_2$|LSC was treated under the same conditions as the composites (air, 1350 °C for 5 h). After high-temperature treatment this system contains two spatially separated interfaces {LSC| modified $CeO_2$} and a modified ceria interlayer. The LSC layers can be considered as the non-blocking electrodes because of high mixed ionic-electronic conductivity. Impedance spectra recorded for the three layered system at 500 °C are presented in Figure 10. The electrical behavior of the LSC|$CeO_2$|LSC system is noticeably different on heating (ICS) and cooling (HCS), showing hysteretic behavior similar to that for LSCC57-R007, LSCC57-P008 and LSCC57-M001 composites (Figures 1 and 10). So, the origin of the conductivity hysteresis observed in the LSCC57-R007, LSCC57-P008, and LSCC57-M001 composites can be directly related to the transport properties of the chemically modified phase interface.

Two processes contribute in the total impedance of the three layered system: the high and low frequency processes (Figure 10). Parameters obtained from the fitting of the impedance spectra are presented in Table 4. In the present study we would like to discuss the high frequency relaxation process because it contributes mainly to the total impedance of the three layered system and shows the strongest difference in the HCS and ICS. The $C_H$ (Table 4) recalculated with the consideration of the geometrical factors ($C_H^{Geom}$) is 1 order of magnitude lower of 1 pF/cm, which is typical for the bulk contribution.[56] Microstructural analysis showed that the interlayer of 22 $\mu$m in thickness is slightly porous

**Table 4. Parameters Obtained from the Fitting of the Impedance Spectra Collected at 500 °C on Heating and Cooling for the LSC|$CeO_2$|LSC Three Layered System (Figure 10)**

| | high frequency arc | | | | |
|---|---|---|---|---|---|
| time, h | $R_H$, kOhm | $C_H$, F | $R_{CT}$, Ohm | $C_{INT}$, F | $Z_W$ kOhm |
| | | Heating up (ICS) | | | |
| 0 | 4.85 | $1.83 \times 10^{-10}$ | 236.1 | $3.31 \times 10^{-7}$ | 1.42 |
| 10.7 | 4.63 | $1.82 \times 10^{-10}$ | 238.4 | $3.39 \times 10^{-7}$ | 1.50 |
| 12 | 4.63 | $1.81 \times 10^{-10}$ | 262.9 | $4.17 \times 10^{-7}$ | 1.66 |
| | | Cooling down (HCS) | | | |
| 0 | 2.59 | $1.63 \times 10^{-10}$ | 95.4 | $6.15 \times 10^{-7}$ | 1.21 |
| 9.2 | 2.76 | $1.66 \times 10^{-10}$ | 101.9 | $4.21 \times 10^{-7}$ | 1.49 |
| 12 | 2.79 | $1.66 \times 10^{-10}$ | 119.8 | $4.96 \times 10^{-7}$ | 1.44 |

and composed of micro- and nanosized particles, indicating complex morphology. SEM/EDX confirmed the presence of La, Sr, and Co in the middle of the ceria interlayer, presuming spontaneous penetration and chemical interaction during co-firing the system at 1350 °C, like for LSCC57 composites. XRD analysis carried out in reflection mode at the surface of the LSC pellet covered by the ceria interlayer (from the three layered system) showed the presence of a series of highly disordered solid solution with fluorite structure ($Fm\bar{3}m$) with different lattice parameters ($a$ = 5.5207(1) Å, $a$ = 5.4817(1) Å, and $a$ = 5.4370(1) Å), a phase with triclinic structure formally corresponding to $Ce_{11}O_{20}$, which is similar to that observed in LSCC57-R007 and LSCC57-P008 powders by TEM at the nanoscale, and a phase with fluorite structure ($Fm\bar{3}m$) with $a$ = 5.4176(1), which is very close to that for $CeO_2$ as an individual phase (Table 1). Notice that if the lattice parameter of the modified ceria equals to 5.5207(1) Å, it corresponds formally to the dissolution of up to 30 mol % La in the fluorite structure; ~20 mol % La for $a$ = 5.4817(1) Å and ~6 mol % La for $a$ = 5.4370(1) Å).[42] According to XPS, however, La, Sr, and Co cations are present on the surface in the comparable concentrations: 4.1, 4.1, and 3.5 at. %, respectively. The concentrations of Ce and O are equal to 11.9 and 76.4 at. %, respectively. Moreover, the fundamental studies showed[42,57] that the total conductivity of cations doped $CeO_2$ are higher compared to undoped $CeO_2$, although values of conductivity vary significantly depending on chemical nature of dopants, their concentration, and oxidation state. For instance, the conductivity of $Ce_{0.7}La_{0.3}O_{2-\delta}$ equals to

(56) Irvine, J. T. S.; Sinclair, D. C.; West, A. R. *Adv. Mater.* **1990**, *2*, 132.

(57) Mogensen, M.; Lindegaard, T.; Hansen, U. R.; Mogensen, G. *J. Electrochem. Soc.* **1994**, *141*, 2122.

$2.5 \times 10^{-2}$ S/cm at 800 °C.[42] In the present study we found that the bulk conductivity of the single phase LSCC92.4 is higher by 4 orders of magnitude compared to $CeO_2$ at 508 °C and also shows the difference in the value of conductivity on heating and cooling: $\sigma_{(ICS)} = 1.2 \times 10^{-2}$ S/cm and $\sigma_{(HCS)} = 3.0 \times 10^{-2}$ S/cm. In the case of the LSCC89.4, the difference in the conductivity on heating and cooling was also observed: $\sigma_{(ICS)} = 5.6 \times 10^{-2}$ S/cm and $\sigma_{(HCS)} = 1.96 \times 10^{-1}$ S/cm. Considering complex morphology and phase composition within the modified interlayer, one can presume that an effective geometrical factor used for the recalculation of $C_H$ should be much less. This might indicate also that the brickl model[58] traditionally used for the description of the transport properties of polycrystalline systems is not applicable, assuming that effective conduction paths within the modified ceria interlayer could be located through thin films of the most conductive phases formed on the surface or between grains of modified ceria and could be governed by different types of low-dimensional percolation behavior.

## 4. Conclusions

At room temperature all 43 mol % $La_{0.6}Sr_{0.4}CoO_{3\pm\delta}$·57 mol % $CeO_2$ (LSCC57) composites fabricated in different ways are composed of the modified perovskite with rhombohedrally distorted perovskite structure ($R\bar{3}c$, no. 167) and modified ceria with fluorite structure ($Fm\bar{3}m$, no. 225). The modification of the initial components takes place because of cross-solubility of La, Sr, and Co from $La_{0.6}Sr_{0.4}CoO_3$ in the fluorite structure and solubility of Ce in the perovskite structure. However, transport properties of the LSCC57 composites vary drastically. The LSCC57 composites show similar high conductivity on heating and cooling, if there is good connectivity between grains of the modified perovskite. Nano scale phase transformations, which are different from those observed at the macro scale, seem to not affect conductivity of the LSCC57 composites in this case. Nevertheless, the electronic conductivity in the composite materials could be suppressed because of recombination of holes (from the modified perovskite) and electrons (from the modified ceria) at the phase interfaces.

In the case of insufficient connectivity between the grains of the modified perovskite the role of chemical interactions and structural coherence at the phase interface become important. Spontaneous chemical interactions taking place at phase interfaces in the LSCC57 composites during high temperature treatment could lead to a formation of anion deficient Ce-containing phases with variable degree of multication substitution (for La, Co, and Sr); and, as the consequence, with different value of conductivity. If grains of the modified perovskite do not form a 3D continuous medium through the composite material for charge and mass transfer, effective conduction pathways could be located along phase interfaces and within nano scale phases spontaneously formed at phase interfaces. Strong reversible conductivity hysteresis between heating and cooling cycles observed for the LSCC57 composites could be related to specific behavior of chemically modified phase interfaces LSC/$CeO_2$ or co-doped $CeO_2$.

**Acknowledgment.** The authors gratefully acknowledge Engineering and Physical Sciences Research Council for the financial support and Dr. S. M. Francis for XPS measurements.

**Supporting Information Available:** XRD patterns of LSCC57-M001, LSCC57-P008, LSCC57-R100, and LSCC57-R261; XRD patterns of single phase solid solutions LSCC92.4 and LSCC88; SEM images of LSCC57-R007 and LSCC57-P008 with detail on distribution of the modified perovskite and ceria; comparison of the thermal expansion and conductivity on heating and cooling in LSCC57-R007; TEM images of the particle with a large amorphous region, containing nanosize $CeO_2$ inclusions in LSCC57-R048. This material is available free of charge via the Internet at http://pubs.acs.org.

(58) Bauerle, J. E. *J. Phys. Chem. Solids* **1969**, *30*, 2657.